ELECTROPOLYMERIZED POLYAZULENE AS ACTIVE MATERIAL IN FLEXIBLE SUPERCAPACITORS

Milla Suominen[a], Suvi Lehtimäki[b], Rahul Yewale[a], Pia Damlin[a,*], Sampo Tuukkanen[c], Carita Kvarnström[a]

[a]Turku University Centre for Materials and Surfaces (MATSURF), Laboratory of Materials Chemistry and Chemical Analysis, University of Turku, FIN-20014 Turku, Finland

[b]Department of Electronics and Communications Engineering and [c]Department of Automation Science and Engineering, Tampere University of Technology, FIN-33720 Tampere, Finland

[*]Corresponding author. E-mail: pia.damlin@utu.fi (Pia Damlin), Tel.: +358 50 328 5468, Fax: 029 450 5040

Abstract

We report the capacitive behavior of electrochemically polymerized polyazulene films in different ionic liquids. The ionic liquids in this study represent conventional imidazolium based ionic liquids with tetrafluoroborate and bis(trifluoromethylsulfonyl)imide anions as well as an unconventional choline based ionic liquid. The effect of different ionic liquids on the polymerization and capacitive performance of polyazulene films is demonstrated by cyclic voltammetry and electrochemical impedance spectroscopy in a 3-electrode cell configuration. The films exhibit the highest capacitances in the lowest viscosity ionic liquid (92 mF cm^{-2}), while synthesis in high viscosity ionic liquid shortens the conjugation length and results in lower electroactivity (25 mF cm^{-2}). The obtained films also show good cycling stabilities retaining over 90 percent of their initial capacitance over 1200 p-doping cycles. We also demonstrate, for the first time, flexible polyazulene supercapacitors of symmetric and asymmetric configurations using the choline based ionic liquid as electrolyte. In asymmetric configuration, capacitance of 55 mF (27 mF cm^{-2}) with an equivalent series resistance of 19 Ω is obtained at operating voltage of 1.5 V. Upon increasing the operating voltage up to 2.4 V, the capacitance increases to 72 mF (36 mF cm^{-2}).

Keywords: electropolymerization, polyazulene, ionic liquid, choline, flexible supercapacitor

1. Introduction

Electrochemical double-layer capacitors (EDLCs) or supercapacitors have been developed as fast energy delivering systems for electric vehicles and small electronics. Their energy storage mechanism relies on a fast and highly reproducible formation of an electrochemical double-layer in the near vicinity of highly porous activated carbon electrodes which is why they offer the advantage of longer device lifetimes and faster charging/discharging rates than batteries [1]. In addition, eco-friendlier materials and simpler manufacturing methods such as printing can be applied to construct EDLCs [2–4]. However, the energy density of

supercapacitors needs to be increased, and therefore graphene [5–7], carbon nanotubes [2,8], and pseudocapacitive substances have gained an increasing attention as promising electrode materials in supercapacitors.

Electronically conducting polymers (ECPs) are an intriguing choice of material due to low cost, good conductivities, simple and easy fabrication methods, and extensive possibilities to modify their structure. ECPs, for example, can be easily functionalized to produce better soluble materials suitable for fabricating devices with roll-to-roll technique [9]. ECPs are also flexible in nature and have good tensile strengths which is why they have aroused interest in bendable electronics and textiles [10,11]. ECP-based devices can store more energy than conventional EDLCs since the energy is not only stored in the electrical double layer at the electrode surfaces but mostly in the fast Faradaic processes which take place in the bulk material. These reactions require counter ions from the electrolyte to diffuse into the polymer film to maintain charge neutrality which causes the film to swell and shrink during operation. Quite quickly it became obvious that this swelling and shrinking was devastating for the polymer film's long term cycling stability. Several improvements for this problem have been suggested including fabricating ECPs together with different carbonaceous media [3,12–14], modifying the structures of the monomers [9] and changing the electrolyte from conventional organic and aqueous solutions to ionic liquids (ILs) [15–18].

ILs have been extensively studied as electrolytes in electrosynthesis of ECPs and in supercapacitors. On both occasions, the use of ILs has resulted in better performances; using them in polymerization results in increased electrochemical activity, conductivity and porosity of ECP films [19–23], whereas an increase in long term cycling stability of ECP supercapacitors has been reported on numerous occasions [15–18,24,25]. It has also been stated, that ILs enables the manufacturing of safer energy storage because they have low volatilities and negligible vapour pressures compared to organic solvents. However, when heated, ILs can produce toxic gases [26] and conventional ILs bio-accumulate and form eco-toxic compounds according to several biodegradation studies [27]. This has lead chemists to design new, less hazardous ionic solvents, and not so surprisingly, they have mimicked nature by using biomolecules such as choline, amino acids, and other small organic acids as the new building blocks for bio-ILs [28–31]. The use of imidazolium based ILs still exceeds that of the new biodegradable choices, probably because of high viscosities and hygroscopic nature of bio-ILs, but there are some examples on the use of choline-based molten salts in energy storage applications in literature [32]. ECP's properties depend on the type of electrolyte and solvent used, and the effect of bio-ILs on ECPs and ECP-based devices should be studied and further compared to conventional ILs.

Another method of improving ECP supercapacitors is to focus on new polymer materials. Among the vast conducting polymer family, polyaniline (PANi), poly(3,4-ethylenedioxythiophene) (PEDOT), and polypyrrole (PPy) have received most attention as supercapacitor materials. The first one mostly due to its high intrinsic

capacitance [33] while the other two have shown better tolerance towards long term cycling [25]. Azulene, a non-benzenoid aromatic hydrocarbon with fused five and seven membered rings in its structure, can be polymerized to produce highly conductive polyazulene (PAz) films [34]. PAz has recently been deemed a well-suitable ion-to-electron transducer material for all-solid-state ion selective electrodes due to its high charging capacity [35] and, owing to the unique charge distribution between the rings, azulene has distinctive electron donating properties that can be utilized in dye sensitized solar cells [36,37]. To date, PAz has aroused little attention as a viable supercapacitor material although its specific capacitance in acetonitrile has been determined to be as high as 400 F g^{-1} [38] which is very close to the specific capacitance of PANi [33]. Few earlier studies have established the differences between the polymerization and electroactivity of PAz in different organic solvents [38,39] as well as between acetonitrile and a pyrrolidinium based IL [23], but to our knowledge the effect of using different types of ILs to study its capacitive behaviour has not been reported. Additionally, the capacitances reported so far have all been measured in a 3-electrode configuration, but assembled supercapacitor devices based on PAz have not been fabricated and studied.

This work presents how different ILs affect the polymerization, morphology and electrochemical activity of PAz. The viscosity and the ions constituting the ILs were found to be important factors in obtaining good electroactivity. Two conventional imidazolium based ILs, (1-ethyl-3-methylimidazolium bis(trifluoromethylsulfonyl) imide [Emim][TFSI] and 1-hexyl-3-methylimidazolium tetrafluoroborate [Hmim][BF_4]), were chosen and compared against choline bis(trifluoromethylsulfonyl)imide [Choline][TFSI]. The films were polymerized on different substrates with cyclic voltammetry (CV) followed by determining their electrochemical activity using CV and electrochemical impedance spectroscopy in a 3-electrode configuration. In this configuration, the capacitances ranged from 25 to 92 mF cm^{-2}, which are close to the values reported for PAz [35] and PANi [14] electropolymerized in acetonitrile. The films retained over 90 % of their capacitance during long term cycling in ambient conditions reaching similar values to what we have previously reported for PEDOT and PEDOT/rGO composites in ILs [10]. Finally, PAz was polymerized on flexible substrates, and symmetric and asymmetric supercapacitors were assembled using the choline-based IL as electrolyte. Blade coated activated carbon functioned as negative electrode in the asymmetric configuration, and galvanostatic charging and discharging was applied to study the device performance. In asymmetric configuration, operating voltages up to 2.4 V could be reached obtaining a capacitance of 72 mF (36 mF cm^{-2}). These values exceed those we have previously presented for flexible PEDOT and PEDOT/rGO devices [10].

2. Experimental

2.1 Materials

Ferrocene (Aldrich, 98 %), azulene (Aldrich, 99 %), 1-hexyl-3-methylimidazolium tetrafluoroborate [Hmim][BF_4] (Iolitech, 99 %), 1-ethyl-3-methylimidazolium bis(trifluoromethylsulfonylimide) [Emim][TFSI] (Iolitech, 99 %), and choline bis(trifluoromethylsulfonyl)imide [Choline][TFSI] (Iolitech, 99 %) were all used as received. ILs were stored in argon filled glove box, while ferrocene and azulene were stored in ambient conditions. Ferrocene and azulene were used as received, and all ILs were dried in vacuum oven (80 ºC) for 2 h and deaerated with dry N_2 for 15 min prior to use.

2.2 Electrode preparation

Ag/AgCl pseudo reference electrode served as reference electrode in all electrochemical measurements. The potential of the reference electrode was calibrated vs. ferrocene (Fc^0/Fc^+) before every measurement ($E_{Fc/Fc+}$ = 0.11 V). Pt-minielectrode (⌀ 1 mm, capacitance in 3-electrode configuration and impedance), tin oxide glass (SnO_2) (⌀ 5 mm, spectroscopic analysis), indium doped tin oxide glass (ITO) (UV-Vis analysis) and poly(ethylene terephthalate) (PET) with silver and graphite ink as conducting layer (⌀ 1.4 cm, current collector electrodes) were used as working electrodes depending on application mentioned in parenthesis. Pt-minielectrode was subsequently polished mechanically with diamond pastes from 3 to 0.25 µm (Struers A/s) and carefully rinsed with quartz distilled water and ethanol between different pastes and before use. SnO_2 (K Glass from Pilkington, sheet resistance = 8.1 Ω cm^2) and ITO glass substrates (Fused quartz glass from Delta Technologies with R_S = 10-20 Ω, 7 x 50 x 1 mm in size) were cleaned by ultrasonication in acetone, ethanol and quartz distilled water successively for 10 min. Current collector electrodes were prepared on PET (Melinex ST506, Dupont Teijin Films) according to a procedure reported earlier [10].

2.3 Electrosynthesis procedure

Azulene was electrochemically polymerized from different ILs containing either imidazolium or cholinium cation and tetrafluoroborate or triflimide anion using two monomer concentrations, 20 and 50 mM, and two temperatures, 20 ºC (room temperature) and 32 ºC. Polymerizations in [Choline][TFSI] were always conducted at 32 ºC due to problems with solidification near room temperature and in [Emim][TFSI] and [Hmim][BF_4] both temperatures were studied. Films were prepared using cyclic voltammetry technique where the potential was cycled between -0.7 and 1.1 V at 50 mV s^{-1} scan rate. CV was chosen as polymerization technique since film formation can be easily controlled by this method. For supercapacitor assembly, films were polymerized using a potential range -0.7−0.9 V at 20 mV s^{-1} scan rate due to substrate restrictions.

2.4 Electrochemical characterization

After polymerization, the deposited films were rinsed with monomer-free IL to remove monomer and oligomer residues. The films were then placed in neat IL and CV response of the films was studied using two potential ranges, -0.6−0.8 V and 0.0−0.8 V, at several scan rates (20, 50, 100, 150 and 200 mV s^{-1}). In long term cycling test, 1200 cycles in the potential range 0.0−0.8 V at 100 mV s^{-1} scan rate was applied. In all CV experiments, a Metrohm Autolab PGSTAT101 potentiostat and a conventional 3-electrode configuration were used. Impedance spectra were attained using IviumStat potentiostat. The spectra were acquired every 100 mV in the potential range -0.5−0.7 V. In the frequency range 100 kHz−100 mHz, 99 frequencies with an amplitude of 10 mV was applied. Impedance was measured directly after polymerization and long term cycling. Electrochemistry was performed at 32 ºC due to solidification of [Choline][TFSI] near room temperature.

Devices of both symmetric and asymmetric configurations were assembled. In asymmetric configuration, activated carbon (AC) was used as anode material. Layers of size 1.4 cm x 1.4 cm were blade-coated through a tape mask from an AC ink prepared from Kuraray YP-80F, chitosan, acetic acid and water (described in detail in [40]). The dry mass of the AC layer was 5 mg. In the symmetric configuration, two similar PAz electrodes were used. A paper separator (Dreamweaver Silver AR25) was used, and supercapacitors were assembled with adhesive film- and tape sealing. The assembly as well as the measurements were conducted inside an argon-filled glove box.

During the measurements, the sample was kept on a hotplate at 35 °C with a small weight on top of the active area. A Maccor 4300 battery test system was used in the characterization. The capacitance was determined from a galvanostatic discharge at 1 mA after a 30-minute voltage hold through C = I/(dV/dt) between 80% and 40% of the maximum voltage. The equivalent series resistance (ESR) was determined from the initial IR drop of a galvanostatic discharge at 10 mA after a 30-minute voltage hold at 1.5 V. Additionally, CV curves were recorded at 100, 50, 10 and 5 mV s^{-1}.

The flexibility of the supercapacitors was examined by wrapping the device on a metal cylinder and measuring the capacitance with the device on the hotplate. Two cylinder radii were used: 1.85 cm and 1.5 cm. The effect of the maximum voltage was also tested: the capacitor was charged to 1.8 V, 2.1 V and 2.4 V, holding each voltage for 30 minutes before galvanostatic discharge at 1 mA. Charge-discharge curves were recorded at 1 mA with the different maximum voltages.

2.5 Structural characterization

For IR and SEM, the films were polymerized over 15 potential cycles on SnO_2 glass. IR spectra were recorded with Bruker Vertex 70 FTIR spectrometer. The spectra were acquired using a Harrick Seagull variable angle reflection accessory and liquid nitrogen cooled MCT detector. The spectra were measured at 55º angle of incidence relative to the surface normal with 4 cm^{-1} spectral resolution. For each spectrum 124 scans was

recorded. SEM images were recorded using LEO (Zeiss) Gemini 1530 FEG-SEM. For UV-Vis, films were polymerized on ITO coated glass, and the measurements were carried out by Cary 60 spectrophotometer (Agilent Technologies).

3. Results and discussion

3.1 Optimizing the electropolymerization procedure in different ionic liquids

Representative multicycle voltammograms recorded during polymerization of 50 mM azulene in different ILs at 32 ºC are presented in Fig. S1. In all studied conditions, a continuous increase of the current with each cycle is observed indicating that an electroactive film forms on the electrode. In the first cycle, trace crossing is detected in the imidazolium based ILs while in [Choline][TFSI] the nucleation loop is not perceived. The absence of trace-crossing in IL media has been previously explained as stabilization of oligoazulene cations by ion-association in ILs which prevents, to some extent, the comproportionation reactions between charged and neutral species [23]. Monomer oxidation as well as polymer oxidation and reduction take place at slightly higher potentials in [Hmim][BF_4] compared to [Emim][TFSI] and [Choline][TFSI] (Table 1). This can be attributed to the higher viscosity of [Hmim][BF_4] which results in slower transport kinetics [20,21]. Additionally, a shift in the oxidation peaks and the onset potential of polymer oxidation towards more anodic values during the course of polymerization is detected in [Hmim][BF_4]. In [Emim][TFSI] and [Choline][TFSI], the oxidation response is broad throughout the polymerization and a remarkable shift of redox responses is not detected. In general, our CVs resemble previous studies conducted with other ILs [23] and organic solvents [35,38,42] well.

Some dissimilarities are observed in monomer oxidation and polymer deposition rates due to differences in viscosities and the ions constituting the electrolytes. The peak current density of monomer oxidation (j_{ox}) and total amount of charge accumulated during polymerization (Q_p) are depicted in Table 1 as well as Fig S2. It is evident, that polymerization is the fastest in [Emim][TFSI] at both monomer concentrations. The deposition rate in [Choline][TFSI] is only slightly faster compared to the deposition rate in [Hmim][BF_4], when using 20 mM monomer concentration, but the difference between these systems is increased with the increasing monomer concentration. In fact, polymerization rate of 50 mM azulene in [Choline][TFSI] is similar to the rate in [Emim][TFSI]. However, j_{ox} is notably lower in [Choline][TFSI] than in the other studied ILs. Changing the temperature has no significant effect on the deposition rates in [Hmim][BF_4] while in [Emim][TFSI] a dramatic decrease in the deposition rate is observed when 20 mM azulene is polymerized at 32 ºC whereas the deposition rate is not affected in the 50 mM case.

It is widely accepted that polymerization rate is affected by the convection of reactive species in the near vicinity of the electrode surface, but solvent system and electrolyte ions also have an effect on the polymerization and the

resulting film quality. Grodzka et al. [38] and Iwasaki et al. [39] have studied the polymerization and electrochemical performance of PAz in several organic solvents. Their studies suggest that films of higher electrochemical activity are obtained in solvents with low dielectric constants. Usually, ILs are considered polar solvents since they constitute of ions but ILs combining the imidazolium cation and TFSI anion have actually been shown to have only moderate polarity [42,43]. In addition, interactions between the ions constituting the ILs and the solutes are complex [44]. Österholm et al. [23] compared PAz films electropolymerized in acetonitrile to those fabricated using N,N-butyl-methyl-pyrrolidinium triflimide as reaction medium. The polymerization was found to be much slower in the IL due to differences in solvation of the reactive species which affects the rate for deprotonation.

Azulene solvation in imidazolium ILs could be better due to π-π interactions between the monomer and the cation. Previously, C-H−π interactions have been observed between imidazolium and tetraphenylborate [45] and a stabilization of radical anions due to π-π interactions with imidazolium has been observed when reducing benzaldehyde [46]. Solvation of reactive species affects the activation energy of the coupling reactions and, on the other hand, the deprotonation rate of the monomer is slower in presence of the TFSI anion due to its lower basicity [23]. Therefore, the monomer oxidation is faster in the imidazolium ILs because of better solvation of the monomer. Since the viscosity of [Hmim][BF_4] (314 cP at 20 ºC and 177 cP at 30 ºC [47]) is significantly higher than the viscosity of [Choline][TFSI] (93 cP at 30 ºC [48]) it is safe to assume that more reactive species diffuse in the near vicinity of the electrode in the latter IL. This implication is supported by the fact that polymerization is the fastest in the lowest viscosity IL (viscosity of [Emim][TFSI] is 38 cP at 20 ºC and 27 cP at 30 ºC [49]). Also, the observed shift in the polymer oxidation in [Hmim][BF_4] could indicate shorter conjugation length which could be a direct result of reactive species deficiency near the electrode surface [39].

Good solvation and changes in viscosities could also explain why polymerization rate of 20 mM azulene decreases upon increasing the temperature in [Emim][TFSI]. Diffusion coefficients in [Emim][TFSI] are inversely proportional to the viscosity [50]. Faster diffusion combined with high solubility of the reactive species could result in the monomer and oligomer moieties diffusing away from the electrode vicinity decreasing the rate for polymerization [23]. In the 50 mM case, however, there is probably an excess of reactive molecules close to the electrode surface which reduces the effect of faster diffusion.

Table 1. Charges accumulated during polymerization (Q_P), monomer oxidation potential ($E_{mon,\ ox}$), polymer reduction and oxidation potentials ($E_{red/ox}$), monomer oxidation current densities (j_{ox}), and redox charges of p-doping (Q_{redox}) and peak potentials of oxidation (E_{pa}) and reduction (E_{pc}) in different ILs.

IL	c_{Az} ***(mM)***	Q_p ***(mC cm^{-2})***	$E_{mon,\ ox}$ ***(V)***	$E_{red/ox}$ ***(V)***	j_{ox} ***(mA cm^{-2})***	E_{pa} ***(V)***	E_{pc} ***(V)***	Q_{redox} ***(mC)***

[Emim][TFSI]	20	299.4	0.50	-0.05/-0.02	1.1	0.17	0.07	0.83
[Emim][TFSI]	50	445.9	0.53	0.00/0.05	1.7	0.10	-0.03	2.03
[Choline][TFSI]	20	122.0	0.54	0.00/0.05	0.5	0.13	0.06	0.33
[Choline][TFSI]	50	421.7	0.52	-0.05/0.05	1.2	0.26	-0.14	1.25
[Hmim][BF_4]	20	83.3	0.62	0.15/0.22	1.3	0.58	0.37	0.16
[Hmim][BF_4]	50	238.2	0.60	0.10/0.20	2.6	0.50	0.17	0.34

After polymerization, the films were rinsed with and immersed into monomer-free dried IL and their p-doping behavior was studied. Fig. S3 illustrates the p-doping responses of PAz films in different ILs after polymerization. The redox charges calculated by integration of the CVs as well as the peak potentials of oxidation (E_{pa}) and reduction (E_{pc}) are presented in Table 1. For 20 and 50 mM concentrations, 15 and 10 consecutive cycles were recorded, respectively, and films were prepared in room temperature in [Emim][TFSI] and [Hmim][BF_4]. The onset potential of oxidation as well as E_{pa} and E_{pc} lie at higher potentials in [Hmim][BF_4] than in [Emim][TFSI] and [Choline][TFSI] which supports the idea of shorter conjugation length [23]. Increasing the monomer concentration raised the polymerization rate and consequently Q_p. If we assume 100 % current efficiency, this results in more deposited material which leads to higher electrochemical activity. This is evident from higher currents (Fig. S3) as well as redox charges (Table 1). Therefore, boosted electrochemical activity of PAz in [Emim][TFSI] is not only due to better conductivity of the electrolyte but also due to thicker films. Thicker films also lead to increased separation of E_{pc} and E_{pa} in all studied electrolytes. This hysteresis phenomenon is least prominent in [Emim][TFSI], while in [Choline][TFSI] thicker films result in clearly separated oxidation and reduction responses. This is mostly caused by higher viscosity and lower ionic conductivity of [Choline][TFSI]. With increasing scan rate (Fig. S4), the potential difference of anodic and cathodic peaks increases slightly in all studied ILs. The largest shifts are observed with the highest viscosity IL which is due to slow ion movement with fast scan rates. Oxidation and reduction peak currents exhibit a nearly linear increase with the increase of square root of the scan rate in all studied systems (Fig. S5) indicating a diffusion controlled electrochemical process occurring in the film, which well-known for thin polymer films.

3.2 Structural characterization

The structures of PAz films polymerized in different media were characterized by scanning electron microscopy (SEM), UV-Vis and IR spectroscopy. The SEM images in Fig. 1 reveal that all films are smooth and evenly distributed over the whole analysis area with granule like structures typical for electropolymerized PAz [23,35,41,51,52]. Slight changes between films polymerized from different ILs are detected. Films prepared in [Choline][TFSI] (Fig. 1a) and [Emim][TFSI] (Fig. 1b) show similar small granule size with well-interconnected 3D network, which has been observed before in organic solvents and other ILs [23,35,52], whereas PAz prepared in [Hmim][BF_4] (Fig. 1c) consists of notably larger granules (roughly 1 µm in diameter) which are widely spread and poorly interconnected. The 3D morphology can be of key importance not only for high power and energy capability of supercapacitors but also for their cycle lives. In conducting polymer films, highly porous structures enables the fluctuation of ions in and out of the film during operation without hindrance. It has been previously written that a smoother and denser morphology of conducting polymers is formed in ILs which facilitates better electrochemical performance [23]. The structure of the films formed in [Choline][TFSI] and [Emim][TFSI] appear smoother and denser than films formed in [Hmim][BF_4] which could partly explain the lower capacitances discussed in the next section.

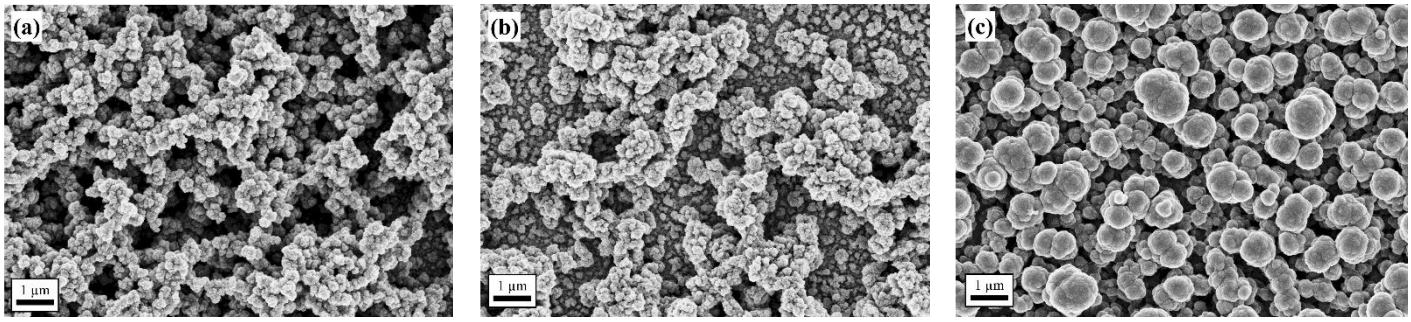

Fig. 1. SEM images of PAz films electropolymerized on SnO_2 glass substrates in (a) [Choline][TFSI], (b) [Emim][TFSI], and (c) [Hmim][BF_4]. Magnifications are 10000x and in a) and c) 50 mM concentration and in b) 20 mM concentration was used.

Based on the CVs and SEM images, a shorter conjugation length in films polymerized in [Hmim][BF_4] was speculated. To gain more insight into the conjugation length of the films, UV-Vis spectroscopy was applied. The UV-Vis spectra of PAz is known to exhibit a broad absorption at around 430 nm due to π-π* transition [41,51] which shifts according to chain length [53]. UV-Vis spectra of undoped PAz films polymerized from different ILs on ITO coated quartz glass are presented in Fig. 2a. PAz in [Emim][TFSI] and [Choline][TFSI] exhibit broad absorption bands tailing to 600 nm with a maximum at 430 nm whereas absorption of PAz in [Hmim][BF_4] has

shifted to slightly lower wavelength (approximately 405 nm) which can be attributed to shorter conjugation [53]. Additionally, the absorption signal of the film prepared from [Hmim][BF_4] is narrower tailing only to around 550 nm which could indicate polymer segments with short conjugation lengths [51].

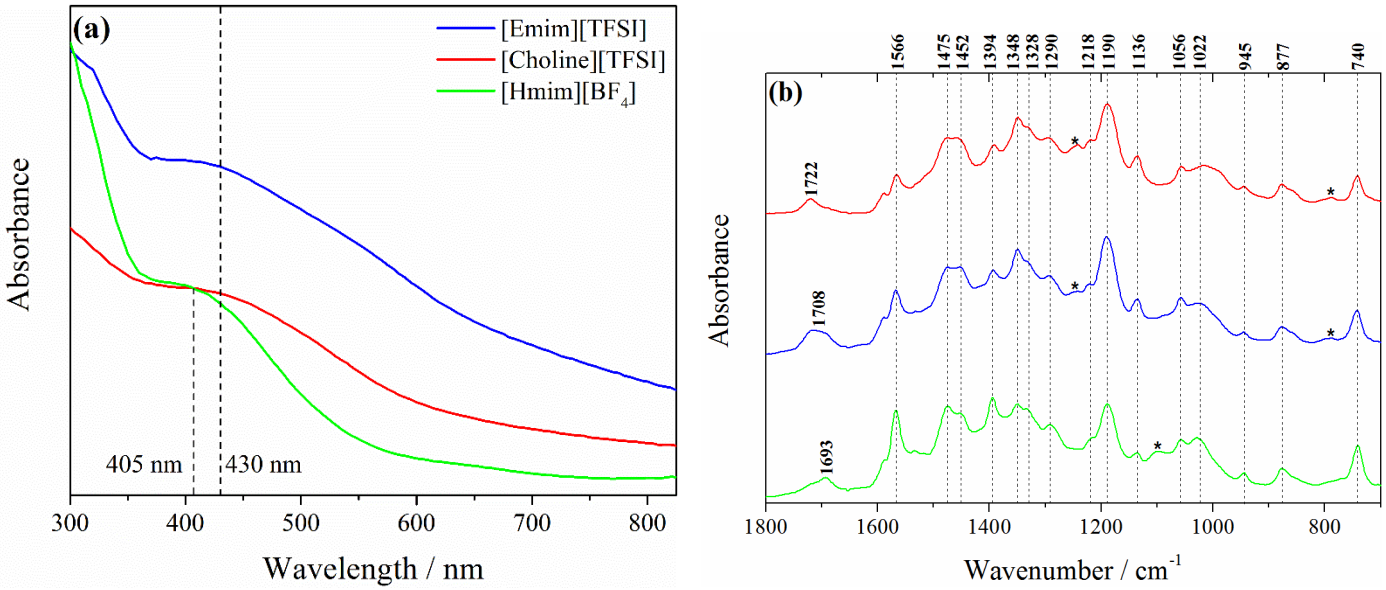

Fig. 2. (a) UV-Vis spectra and (b) IR spectra of PAz films electropolymerized in [Choline][TFSI] (red), [Emim][TFSI] (blue), and [Hmim][BF_4] (green). In (b) the asterisk marks signals from ILs. In (a) the films were formed on ITO coated quartz glass and in (b) SnO_2 glass substrate was used.

The IR spectra show only minor changes due to different counter anions incorporated in the films (Fig. 2b), and are in good agreement with previous findings. IR peaks at 1 566, 1 475, 1 394 and 1 348 cm^{-1} are attributed to the stretching vibrations of C=C bonds [34,51,52,54]. Peaks at 1 452, 1 328 and 1 056 cm^{-1} originate from C-H bending [54]. Out-of-plane deformation vibrations of =C-H are observed at 1 708, 945, 877 and 740 cm^{-1}, and the in-plane deformation vibrations at 1 290, 1 218, 1 190, 1 136 and 1 022 cm^{-1} [34,51,52]. IR bands at 1 245 and 788 cm^{-1} in the spectra of films prepared in [Emim][TFSI] and [Choline][TFSI] are attributed to the counter anion as well as the peak at 1 099 cm^{-1} in the spectrum of PAz in [Hmim][BF_4]. These peaks are designated by an asterisk in Fig. 2b. Additionally, two weak peaks are observed above 1 800 cm^{-1} (3 024 and 3 049 cm^{-1}, not shown) in [Hmim][BF_4] and these bands are attributed to IL residue in the film.

3.3 Capacitance properties in three electrode configuration

In practice, the amount of energy a material is able to store can be estimated by several electrochemical techniques including CV, galvanostatic charging discharging experiments and electrochemical impedance spectroscopy.

Capacitive behavior of PAz in different ILs was first studied using CV and impedance in a 3-electrode cell configuration using the Pt-minielectrode as working electrode while device performance was mainly studied using galvanostatic charging discharging technique. The Q_p was set to 445 mC cm^{-2} to ensure deposition of similar amounts of material. Based on earlier experiments optimizing the electrosynthesis, 50 mM monomer concentration was applied and in [Emim][TFSI] and [Hmim][BF_4] the polymerizations were carried out in room temperature. Fig. 3 depicts the results of cycling the films between 0.0−0.8 V at 20, 50, 100, 150 and 200 mV s^{-1} scan rates. In [Emim][TFSI] (Fig. 3b), an almost ideal rectangular shaped voltammograms are obtained even at the highest scan rates, which indicates fast and efficient doping and dedoping of the polymer material. Upon increasing the scan rate in [Choline][TFSI] (Fig. 3a) and [Hmim][BF_4] (Fig. 3c), deviation from ideality is observed already at low scan rates due to slow ion transfer. High viscosity of [Choline][TFSI] and [Hmim][BF_4] affects the ion transport at fast scan rates. Film thickness, i.e. the amount of material deposited, also has an effect: for thinner films, ideally rectangular shaped CVs are obtained in [Choline][TFSI] at the highest scan rates.

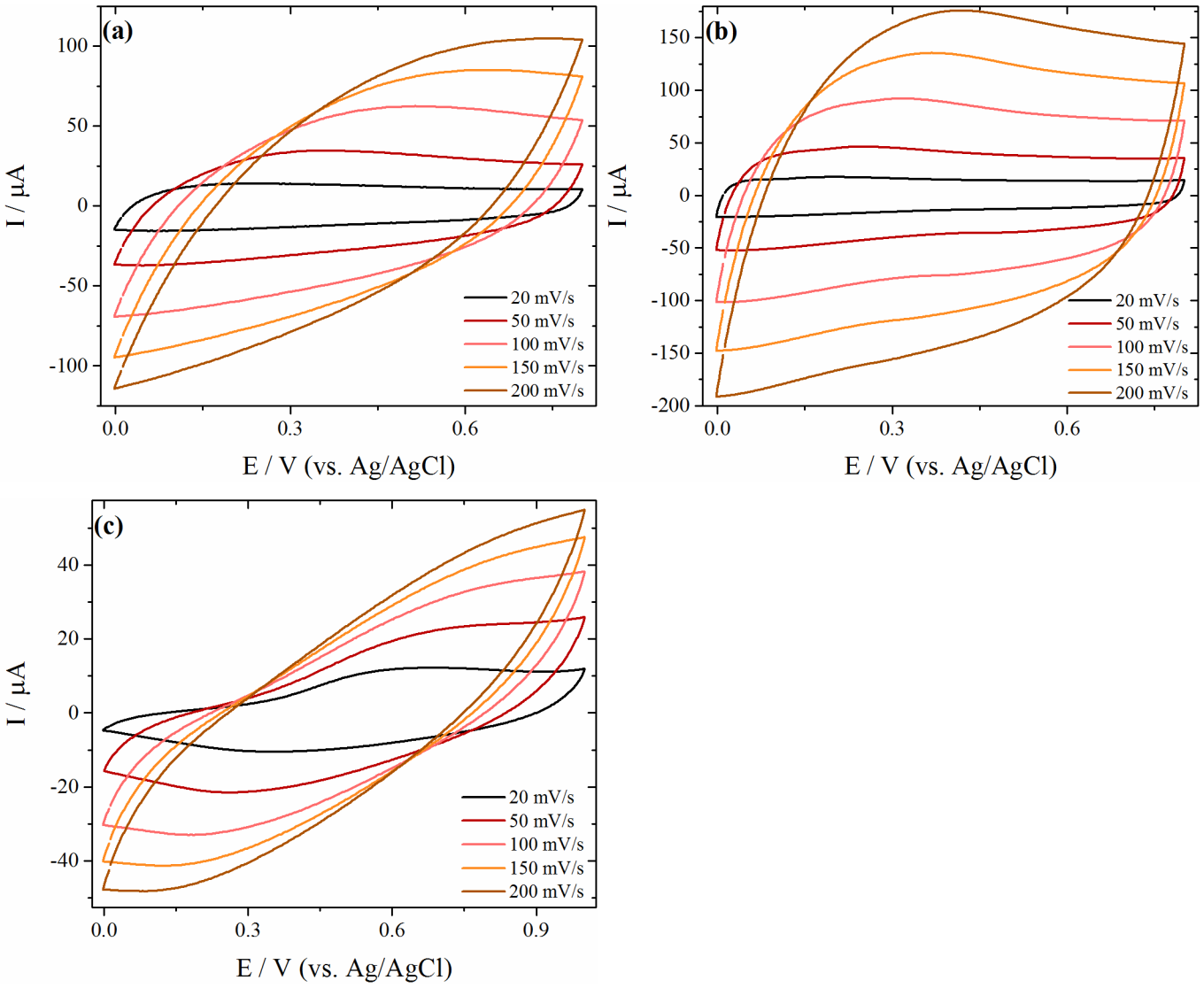

Fig. 3. CVs of PAz electrochemical characterization on Pt electrodes in potential range 0.0−0.8 V at 20, 50, 100, 150 and 200 mV s^{-1} scan rates in (a) [Choline][TFSI] and (b) [Emim][TFSI]. (c) In [Hmim][BF_4] potential range was 0.0−1.0 V.

Capacitances were estimated by integration of the charging half cycle and the dependence of capacitance on scan rate is depicted in Fig. 4a. The highest values are naturally obtained in the lowest viscosity IL and a high capacitance of almost 100 mF cm^{-2} is reached at the lowest scan rate. Also, the capacitance is almost independent of the scan rate in [Emim][TFSI] showing over 80 mF cm^{-2} still at a scan rate of 200 mV s^{-1}. In [Choline][TFSI] and [Hmim][BF_4] capacitances are approximately 70 and 50 mF cm^{-2}, respectively, at the lowest scan rate, but the values decrease quickly when increasing the scan rate and are finally only half of the initial value at 200 mV s^{-1}. The amount of material deposited during polymerization has previously been estimated with Faraday's law [55] assuming a current efficiency of 100 % using equation (1)

$$m = \frac{Q_P * M_{mon}}{nF} \quad (1)$$

In eq. (1), Q_P is the charge accumulated during polymerization (C), M_{mon} is the molecular weight of the monomer (g mol^{-1}), n is the number of electrons, and F is Faraday's constant (96,485.3329 C mol^{-1}). This yields us high specific capacitances of 198 F g^{-1} in [Choline][TFSI], 233 F g^{-1} in [Emim][TFSI] and 86 F g^{-1} in [Hmim][BF_4] when charge is evaluated by integrating the CV obtained using 100 mV s^{-1} scan rate. A maximum specific capacitance of 440 F g^{-1} has been previously estimated by Grodzka et al. [38] using organic solvents with EQCM technique.

Capacitance values are also evaluated by line fitting the dependence of capacitive current on the scan rate [38]. From the slope of I vs. ν in Fig. 4b, the areal capacitance of the films is estimated with equation (2)

$$C = \frac{i}{\nu A} \quad (2)$$

In eq. (2), i is the capacitive current, ν is the sweep rate and A is the area of the electrode (A = 0,00785 cm^2). Estimated capacitances are 63.7 mF cm^{-2} (215 F g^{-1}) in [Choline][TFSI], 112.1 mF cm^{-2} (378 F g^{-1}) in [Emim][TFSI] and 29.2 mF cm^{-2} (98 F g^{-1}) in [Hmim][BF_4]. In acetonitrile, 390 F g^{-1} specific capacitance has been evaluated using this method [38]. Since ILs are more viscous than acetonitrile and therefore should result in lower capacitances, our evaluated values are in good agreement with these previous findings.

Supercapacitors are characterized by their long cycle lives, and ECP based devices have inferior capacitance retention than carbon based devices because of the swelling and shrinking during the doping/dedoping process. Previous studies have suggested that using ILs as electrolytes improves the long term stability of ECP based supercapacitors. Long term cycling stability of the films was studied by applying 1200 p-doping cycles in the range 0.0−0.8 V at scan rate of 100 mV s^{-1}. Fig. 4c presents the capacitance retention of PAz films in different ILs. In [Hmim][BF_4], the films lost generally over 30 % of their electroactivity during the first 800 cycles and,

therefore, were not cycled any further. Currently, 70-80 % capacitance retention is considered sufficient for materials intended for supercapacitor applications [56]. In [Emim][TFSI] and [Choline][TFSI], the films retained over 90 % of their activity after 1200 cycles. In these ILs, slight increase in the capacitance is observed during the first couple hundred cycles which could be explained by reorganization of the polymer matrix. Previously, PAz films have been studied using 250 cycles in organic solvents [38]. In this study, after a steady but slow decrease of the electrochemical activity during the first 200 cycles (-6 %), a dramatic drop in the oxidation charge of the films was observed. This indicates that ILs have an influence on the long term cycling stability of PAz. In the inset of Fig. 4c, the first and last CVs of the long term cycling experiments are shown. In [Choline][TFSI], the most prominent change is the decrease of peak currents whereas in [Emim][TFSI] an anodic shift of the redox potentials is observed. This indicates that the doping process is slightly more reversible in [Choline][TFSI] after long term cycling compared to [Emim][TFSI] [38].

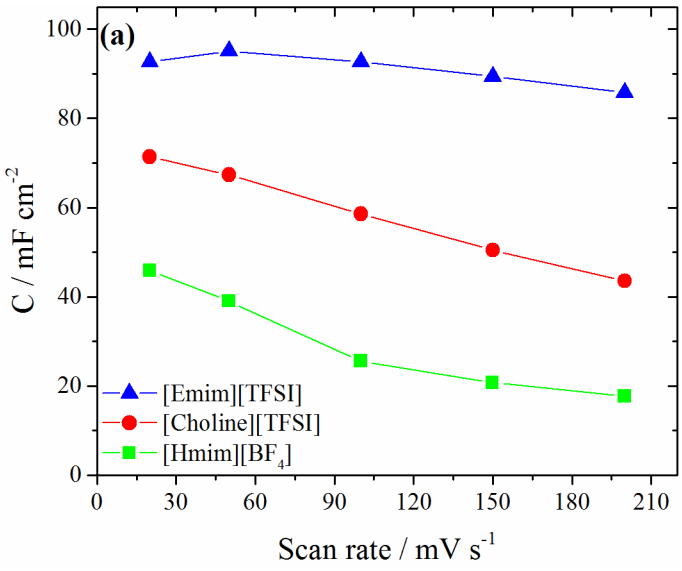

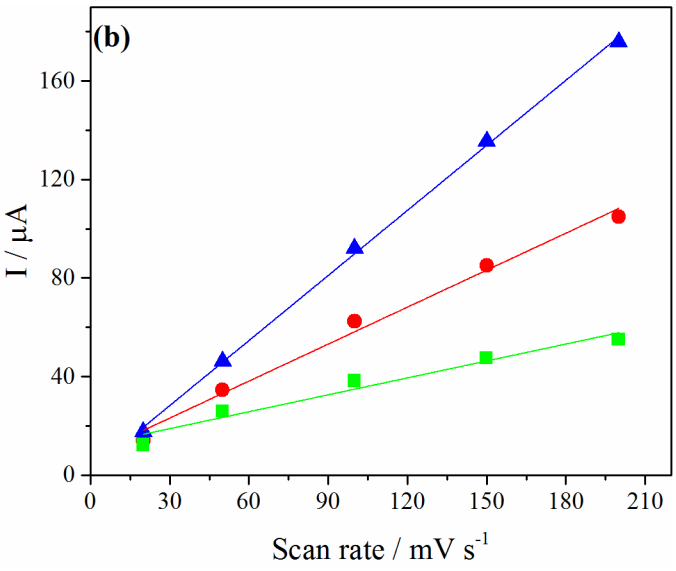

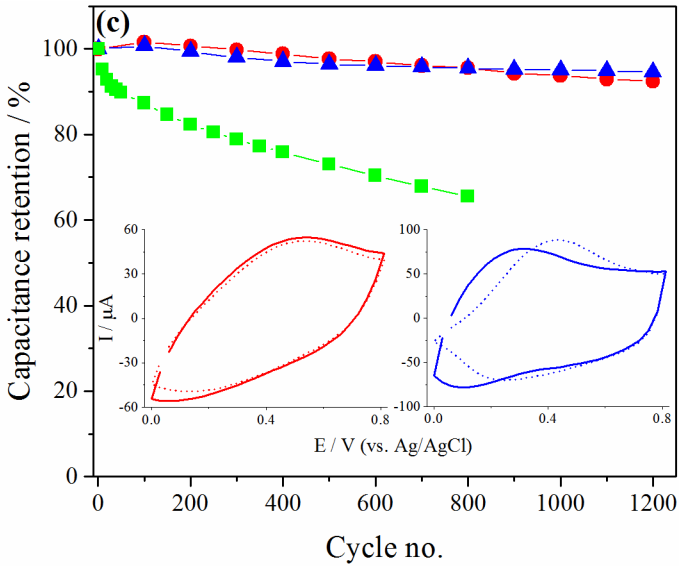

Fig. 4. (a) Dependence of areal capacitance calculated by integration of CVs on the scan rate in different ILs. (b) Dependence of capacitive current on the scan rate in (Δ) [Emim][TFSI], (o) [Choline][TFSI] and (□) [Hmim][BF_4]. (c) Capacitance retention of PAz films in different ILs over long term cycling. The insets show the CVs of the first (solid lines) and 1200th (dashed lines) p-doping cycles of the long term cycling tests. Films were formed on Pt electrodes and studied in 3-electrode configuration.

3.4 Electrochemical impedance analysis of polyazulene films

Electrochemical impedance spectroscopy can be utilized to explain complex interactions between solution/film and film/electrode interfaces, as well as, inside the bulk material. For conducting polymers, the impedance spectra usually exhibit a semi-circle in the high frequency range related to charge transfer resistance (R_{ct}), a linear Warburg diffusion range in the medium frequencies rising at a 45° angle related to diffusion controlled kinetics of the electrode reaction, and a near 90° vertical capacitive line in the low frequency range. Impedance was recorded directly after polymerization and after long term cycling to determine if additional information on the long term cycling effects could be obtained. The results are shown as complex Nyquist plots in Fig 5. and in the supplementary data (Fig. S6 and S7). The solution resistance (R_s) is clearly higher in [Choline][TFSI] than in [Emim][TFSI] indicated by the intersection of x-axis. This is in accordance with the differences in viscosities between these ILs. At potentials < 0 V the impedance response is governed by a large semicircle in both electrolytes. According to CVs, the films are in their neutral form at these potentials, which explains the high R_{ct}. Upon increasing the potential, the films are further doped: the high-frequency semi-circle decreases and distinctive Warburg diffusion and capacitive vertical responses are obtained at low frequencies. Even further doping of the films moves the capacitive response towards higher frequencies and at potentials above 0.3 V Nyquist plots are governed by nearly vertical capacitive lines in both electrolytes.

Some changes in the impeding behavior of the films are evident after long term cycling, depicted in Fig. S6 and S7. In [Choline][TFSI], an increase in the radius of the high frequency semi-circle is detected by naked eye at each measurement potential after long term cycling. In [Emim][TFSI], an increase of R_{ct} is still observed at 0.2 V but as the film is oxidized further, the Nyquist plots of films after polymerization and long term cycling look alike. From the p-doping CVs (Fig. S8) it is obvious that the onset of oxidation has shifted to more anodic potentials in [Emim][TFSI] but the maximum currents have not changed. In [Choline][TFSI], however, both a shift in the potential values as well as a slight decrease in the currents is detected. Increase in resistive behavior can be attributed to changes in the porosity of the film, more precisely to the film becoming more compact in structure making ion diffusion more difficult. Swelling and shrinking of the films over several p-doping cycles could result in denser packing.

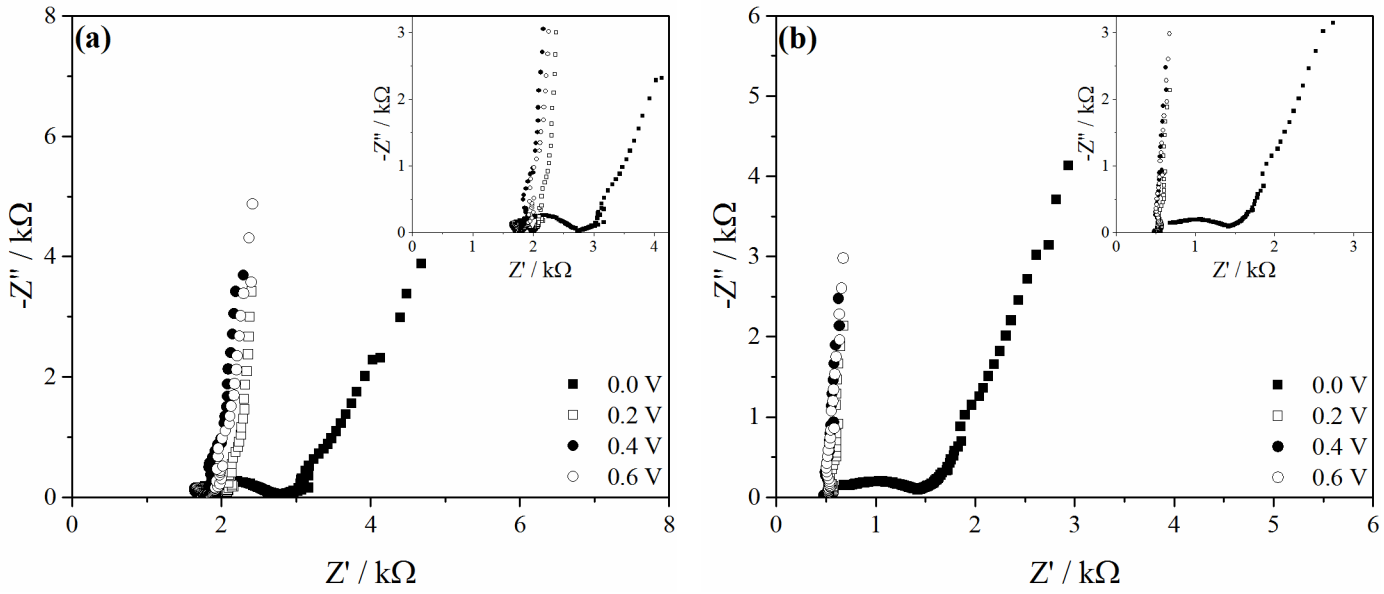

Fig. 5. Complex impedance plots of PAz on Pt electrode in (a) [Choline][TFSI] and (b) [Emim][TFSI] at 0.0, 0.2, 0.4 and 0.6 V. 99 frequencies in the range 100 kHz – 100 mHz with 10 mV amplitude was recorded.

3.5 Performance characteristics of flexible symmetric and asymmetric polyazulene supercapacitors

Studies using 3-electrode configuration give an idea of how the material performs as an energy storage material, but in practice, the materials can behave very differently when applied in a 2-electrode configuration [57]. To better evaluate PAz film's energy storage capabilities, proof-of-concept flexible devices were assembled according to our previous work with PEDOT and PEDOT/rGO composites [10]. Representative multicycle voltammograms of the polymerizations and electrochemical responses in 3-electrode configuration are presented in the supplementary information (Fig. S9).

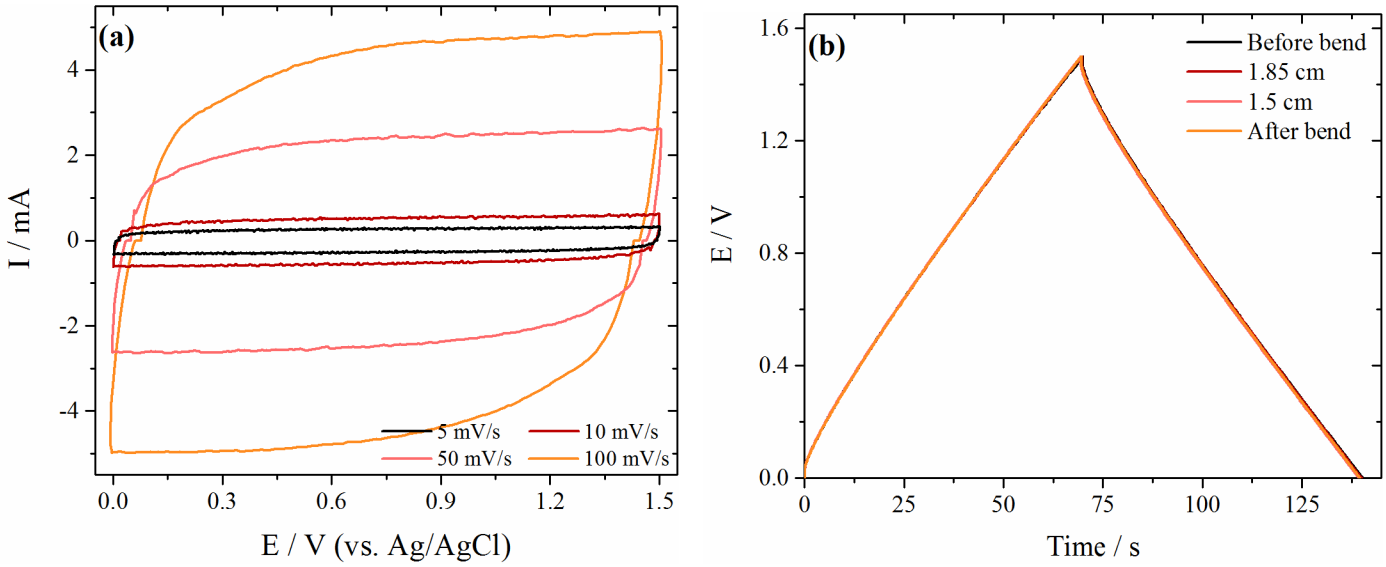

Fig. 6. (a) CVs of a 2 cm^2 supercapacitor on plastic substrate with PAz on the positive electrode and activated carbon on the negative electrode. Slight irregularities at the points where the direction of the current is switched are due to limitations in the measurement system response. (b) Galvanostatic charge-discharge curves at 1 mA of the same supercapacitor sample when bending at radii 1.85 and 1.5 cm, and straightened after the bending.

Supercapacitors were assembled using PAz electropolymerized in [Choline][TFSI] as the positive electrode and activated carbon as the negative electrode. Symmetric devices with PAz on both electrodes were also tested, but the performance was found to be poor; the reason is the undoping of the negative ECP electrode, which results in a loss of conductivity and significant increase in the device resistance [58]. Galvanostatic charge-discharge curves of a symmetric device are shown in Fig. S10. Asymmetric devices had good capacitive performance as can be seen in the CV curves shown in Fig. 6a. The capacitance was measured from a galvanostatic discharge with 1 mA after a 30-minute voltage hold at 1.5 V and the equivalent series resistance (ESR) from the initial IR drop of a similar discharge with 10 mA. The capacitance was 27 mF cm^{-2} for the 2 cm^2 devices, and the ESR 19 Ω. The leakage current, measured at the end of a one-hour voltage hold at 1.5 V, was 1.6 µA. Devices with the PAz layer electropolymerized in [Emim][TFSI] were also prepared, but the properties were similar to those electropolymerized in [Choline][TFSI] due to the activated carbon being the electrode limiting the total capacitance, as is recommended for hybrid supercapacitors [59].

The flexibility of the supercapacitor was demonstrated with a bending test by wrapping the device around a cylindrical tube and measuring the capacitance with the galvanostatic discharge after a 30-minute voltage hold. Cylinders with two different radii were used: 1.85 cm and 1.5 cm. The capacitance decreased 1% from before to after the bending. Galvanostatic charge-discharge curves are presented in Fig. 6b; the curve shape was not changed during the bending.

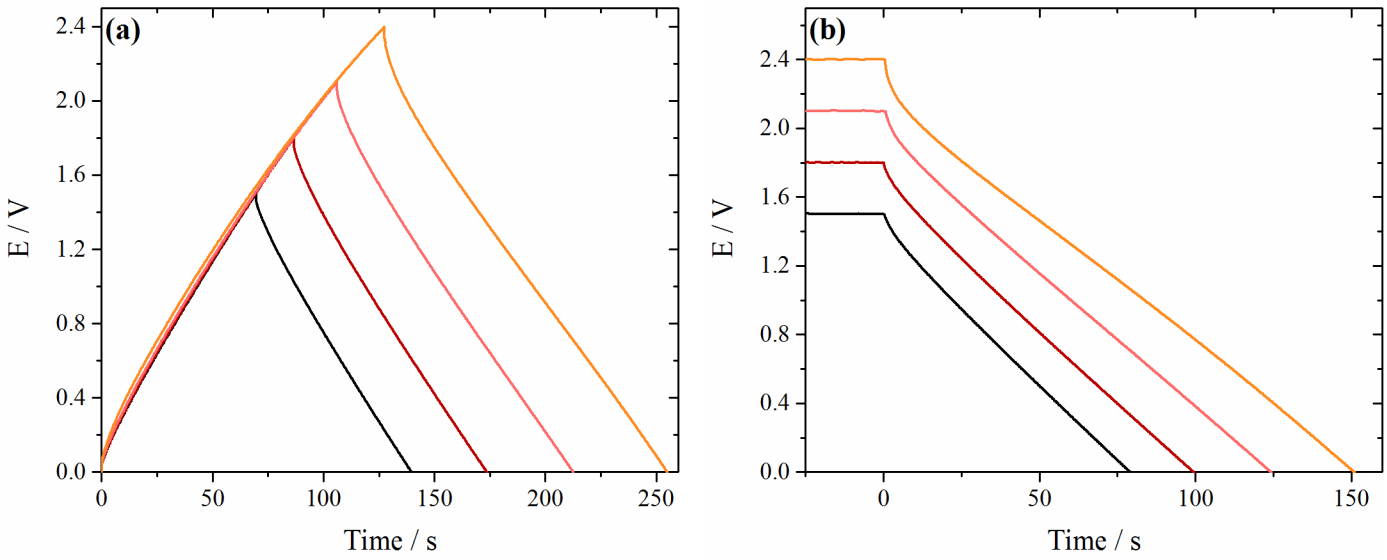

Fig. 7. (a) Galvanostatic charge-discharge and (b) discharge curves after a 30-minute voltage hold at different maximum voltages for the asymmetric flexible supercapacitor with PAz and activated carbon. The current is 1 mA.

Different maximum voltages for the asymmetric flexible supercapacitors were tested up to 2.4 V; the charge-discharge and hold-discharge curves are shown in Fig. 7. The maximum voltage was determined by operating the device at increasing voltages and recording the capacitance and leakage properties as well as observing the charge/discharge curve shape. The capacitance, calculated from the discharge curves after the voltage hold, increased with increasing voltage (Table 2). At 1.8 V, the increase from 1.5 V was 5% but at 2.4 V the increase was 33%. As the energy stored in a capacitor increases also with increasing voltage ($E = ½CV^2$), the resulting increase in energy capacity of the device is 240 %. As seen in Fig. 7, the galvanostatic discharge curves are linear also at the highest voltage, indicating a good capacitive performance. The leakage current increases by an order of magnitude when the voltage is increased from 1.5 V to 2.4 V, indicating that there is a compromise between the higher leakage current and the higher energy given by the increase in operating voltage. The acceptable level of leakage current is determined by the end use application; if the level of 15 µA is acceptable, 2.4 V is an appropriate maximum voltage.

Table 2. Properties of the asymmetric supercapacitor (active area 2 cm^2) calculated from galvanostatic discharge after a 30-minute hold at the maximum voltage. Energy is calculated through $E = ½CV^2$ and the leakage current recorded at the end of the voltage hold.

Voltage (V)	***Capacitance (mF)***	***Energy (mJ)***	***Leakage current (µA)***
1.5	54.7	62	1.5

1.8	57.6	93	5.0
2.1	63.2	139	8.7
2.4	72.6	209	15.8

4. Conclusions

We successfully electropolymerized polyazulene films in different types of ILs. One of the studied ILs incorporated a biodegradable cation and is a step towards greener solvent systems. Viscosity and the ions constituting the ILs proved to affect the polymerization, and the fastest polymerization rates were obtained in the lowest viscosity IL. Using [Hmim][BF_4] as electrolyte resulted in shorter conjugation length of the polymer, and also the morphology of the film was slightly altered. The capacitance of PAz films was evaluated in 3-electrode configuration by integration of p-doping CVs, from the slope of the capacitive current vs. scan rate and from the dependence of imaginary impedance on the reciprocal of frequency. The first two methods yielded very similar capacitances of around 60 mF cm^{-2} in [Choline][TFSI], 90 mF cm^{-2} in [Emim][TFSI] and 25 mF cm^{-2} in [Hmim][BF_4]. Capacitances evaluated from the impedance data resulted in lower values of around 30 mF cm^{-2} in [Choline][TFSI] and 60 mF cm^{-2} in [Emim][TFSI]. The highest values were naturally obtained in the lowest viscosity IL, but the capacitive behavior in [Choline][TFSI] was satisfactory. For PAz polymerized using [Hmim][BF_4] the capacitances were lower, but still similar to those we have previously obtained for PEDOT. The capacitive properties of PAz films are comparable to PANi which so far has been the target of pseudocapacitor studies and has exhibited the highest energy densities among other studied polymers. We also successfully electropolymerized PAz films on a flexible PET-substrate and studied the properties of a flexible PAz-supercapacitor with symmetric and asymmetric configurations. The asymmetric configuration with activated carbon as the negative electrode yielded good capacitive performance up to 2.4 V, where the device capacitance was 36 mF cm^{-2}. The properties of the supercapacitors were not significantly changed through bending down to a radius of 1.5 cm.

Acknowledgements

M.S. acknowledges funding from Doctoral Programme in Physical and Chemical Sciences, and M.S. and R.Y. acknowledge The Real Estate Foundation for financial support. Mauri Nauma is gratefully acknowledged for technical help with cell designs. S.L. thanks the Jenny and Antti Wihuri foundation for supporting the research.

References

[1] R. Kötz, M. Carlen, Principles and applications of electrochemical capacitors, Electrochim. Acta. 45 (2000) 2483–2498.

[2] S. Lehtimäki, S. Tuukkanen, J. Pörhönen, P. Moilanen, J. Virtanen, M. Honkanen, D. Lupo, Low-cost, solution processable carbon nanotube supercapacitors and their characterization, Appl. Phys. A Mater. Sci. Process. 117 (2014) 1329–1334.

[3] J. Keskinen, S. Tuurala, M. Sjödin, K. Kiri, L. Nyholm, T. Flyktman, M. Stromme, M. Smolander, Asymmetric and symmetric supercapacitors based on polypyrrole and activated carbon electrodes, Synth. Met. 203 (2015) 192–199.

[4] F. Pettersson, J. Keskinen, T. Remonen, L. von Hertzen, E. Jansson, K. Tappura, Y. Zhang, C.-E. Wilén, R. Österbacka, Printed Environmentally Friendly Supercapacitors with Ionic Liquid Electrolytes on Paper, J. Power Sources. 271 (2014) 298–304.

[5] Y. Zhu, S. Murali, M.D. Stoller, K.J. Ganesh, W. Cai, P.J. Ferreira, A. Pirkle, R.M. Wallace, K. A. Cychosz, M. Thommes, D. Su, E. A. Stach, R.S. Ruoff, Carbon-based supercapacitors produced by activation of graphene, Science 332 (2011) 1537–1541.

[6] M.D. Stoller, S. Park, Y. Zhu, J. An, R.S. Ruoff, Graphene-based ultracapacitors, Nano Lett. 8 (2008) 3498–3502.

[7] J. Luo, H.D. Jang, J. Huang, Effect of Sheet Morphology on the Scalability of Graphene-Based Ultracapacitors, ACS Nano. 7 (2013) 1464–1471.

[8] Y. Chen, L. Du, P. Yang, P. Sun, X. Yu, W. Mai, Significantly enhanced robustness and electrochemical performance of flexible carbon nanotube-based supercapacitors by electrodepositing polypyrrole, J. Power Sources. 287 (2015) 68–74.

[9] A.M. Österholm, J.F. Ponder, J.A. Kerszulis, J.R. Reynolds, Solution Processed PEDOT Analogues in Electrochemical Supercapacitors, ACS Appl. Mater. Interfaces. 8 (2016) 13492–13498.

[10] S. Lehtimäki, M. Suominen, P. Damlin, S. Tuukkanen, C. Kvarnström, D. Lupo, Preparation of Supercapacitors on Flexible Substrates with Electrodeposited PEDOT/Graphene Composites, ACS Appl. Mater. Interfaces. 7 (2015) 22137–22147.

[11] Y. Huang, H. Hu, Y. Huang, M. Zhu, W. Meng, C. Liu, Z. Pei, C. Hao, Z. Wang, C. Zhi, M. Science, H. Kong, T.C. Avenue, H. Kong, H.C. Road, H. Kong, B. Engineering, H. Kong, T.C. Avenue, H. Kong, H. Kong, From Industrially Weavable and Knittable Highly Conductive Yarns to Large Wearable Energy Storage Textiles, ACS Nano. 9 (2015) 4766–4775.

[12] E. Frackowiak, V. Khomenko, K. Jurewicz, K. Lota, F. Béguin, Supercapacitors based on conducting polymers/nanotubes composites, J. Power Sources. 153 (2006) 413–418.

[13] Z.-F. Li, H. Zhang, Q. Liu, L. Sun, L. Stanciu, J. Xie, Fabrication of high-surface-area graphene/polyaniline nanocomposites and their application in supercapacitors, ACS Appl. Mater. Interfaces. 5 (2013) 2685–2691.

[14] T. Lindfors, R.-M. Latonen, Improved charging/discharging behavior of electropolymerized nanostructured composite films of polyaniline and electrochemically reduced graphene oxide, Carbon 69 (2014) 122–131.

[15] A. Balducci, U. Bardi, S. Caporali, M. Mastragostino, F. Soavi, Ionic liquids for hybrid supercapacitors, Electrochem. Commun. 6 (2004) 566–570.

[16] A. Balducci, W. A. Henderson, M. Mastragostino, S. Passerini, P. Simon, F. Soavi, Cycling stability of a hybrid activated carbon//poly(3-methylthiophene) supercapacitor with N-butyl-N-methylpyrrolidinium bis(trifluoromethanesulfonyl)imide ionic liquid as electrolyte, Electrochim. Acta. 50 (2005) 2233–2237.

[17] A.M. Österholm, D.E. Shen, A.L. Dyer, J.R. Reynolds, Optimization of PEDOT films in ionic liquid supercapacitors: demonstration as a power source for polymer electrochromic devices, ACS Appl. Mater. Interfaces. 5 (2013) 13432–13440.

[18] W. Lu, A.C. Fadeev, B. Qi, E. Smela, B.R. Mattes, J. Ding, G.M. Spinks, J. Mazurkiewicz, D. Zhou, G.G. Wallace, D.R. MacFarlane, S.A. Forsyth, M. Forsyth, Use of Ionic Liquids for Pi-Conjugated Polymer Electrochemical Devices, Science 297 (2002) 983–987.

[19] P.C. Innis, J. Mazurkiewicz, T. Nguyen, G.G. Wallace, D. MacFarlane, Enhanced electrochemical stability of polyaniline in ionic liquids, Curr. Appl. Phys. 4 (2004) 389–393.

[20] J.M. Pringle, M. Forsyth, D.R. MacFarlane, K. Wagner, S.B. Hall, D.L. Officer, The influence of the monomer and the ionic liquid on the electrochemical preparation of polythiophene, Polymer 46 (2005) 2047–2058.

[21] J.M. Pringle, J. Efthimiadis, P.C. Howlett, J. Efthimiadis, D.R. MacFarlane, A.B. Chaplin, S.B. Hall, D.L. Officer, G.G. Wallace, M. Forsyth, Electrochemical synthesis of polypyrrole in ionic liquids, Polymer 45 (2004) 1447–1453.

[22] D. Wei, C. Kvarnström, T. Lindfors, A. Ivaska, Polyaniline nanotubules obtained in room-temperature ionic liquids, Electrochem. Commun. 8 (2006) 1563–1566.

[23] A. Österholm, C. Kvarnström, A. Ivaska, Ionic liquids in electrosynthesis and characterization of a polyazulene-fullerene composite, Electrochim. Acta. 56 (2011) 1490–1497.

[24] D.R. MacFarlane, N. Tachikawa, M. Forsyth, J.M. Pringle, P.C. Howlett, G.D. Elliott, J.H. Davis, M. Watanabe, P. Simon, C.A. Angell, Energy applications of ionic liquids, Energy Environ. Sci. 7 (2014) 232–250.

[25] G. A. Snook, P. Kao, A.S. Best, Conducting-polymer-based supercapacitor devices and electrodes, J. Power Sources. 196 (2011) 1–12.

[26] R.P. Swatloski, J.D. Holbrey, R.D. Rogers, Ionic liquids are not always green: hydrolysis of 1-butyl-3-methylimidazolium hexafluorophosphate, Green Chem. 5 (2003) 361–363.

[27] A. Jordan, N. Gathergood, Biodegradation of ionic liquids - a critical review, Chem. Soc. Rev. 44 (2015) 8200–8237.

[28] W. Gouveia, T.F. Jorge, S. Martins, M. Meireles, M. Carolino, C. Cruz, T. V Almeida, M.E.M. Araújo, Toxicity of ionic liquids prepared from biomaterials., Chemosphere. 104 (2014) 51–56.

[29] X.D. Hou, Q.P. Liu, T.J. Smith, N. Li, M.H. Zong, Evaluation of Toxicity and Biodegradability of Cholinium Amino Acids Ionic Liquids, PLoS One. 8 (2013) e59145.

[30] Q.-P. Liu, X.-D. Hou, N. Li, M.-H. Zong, Ionic liquids from renewable biomaterials: synthesis, characterization and application in the pretreatment of biomass, Green Chem. 14 (2012) 304–307.

[31] J. Pernak, A. Syguda, I. Mirska, A. Pernak, J. Nawrot, A. Prądzyńska, S.T. Griffin, R.D. Rogers, Choline-derivative-based ionic liquids, Chem. - A Eur. J. 13 (2007) 6817–6827.

[32] D. Aradilla, F. Gao, G. Lewes-Malandrakis, W. Müller-Sebert, P. Gentile, M. Boniface, D. Aldakov, B. Iliev, T.J.S. Schubert, C.E. Nebel, G. Bidan, Designing 3D Multihierarchical Heteronanostructures for High-Performance On-Chip Hybrid Supercapacitors: Poly(3,4-(ethylenedioxy)thiophene)-Coated Diamond/Silicon Nanowire Electrodes in an Aprotic Ionic Liquid, ACS Appl. Mater. Interfaces. 8 (2016) 18069–18077.

[33] G.A. Snook, G.Z. Chen, The measurement of specific capacitances of conducting polymers using the quartz crystal microbalance, J. Electroanal. Chem. 612 (2008) 140–146.

[34] F. Wang, Y.H. Lai, N.M. Kocherginsky, Y.Y. Kosteski, The first fully characterized 1,3-polyazulene: High electrical conductivity resulting from cation radicals and polycations generated upon protonation, Org. Lett. 5 (2003) 995–998.

[35] N. He, L. Höfler, R.M. Latonen, T. Lindfors, Influence of hydrophobization of the polyazulene ion-to-electron transducer on the potential stability of calcium-selective solid-contact electrodes, Sensors Actuators B Chem. 207 (2015) 918–925.

[36] R.M. Latonen, C. Kvarnström, A. Ivaska, Electrochemical preparation of oligo(azulene) on nanoporous TiO2 and characterization of the composite layer, J. Appl. Electrochem. 40 (2010) 1583–1591.

[37] R.M. Latonen, A. Österholm, C. Kvarnström, A. Ivaska, Electrochemical and spectroelectrochemical study of polyazulene/BBL-PEO donor-acceptor composite layers, J. Phys. Chem. C. 116 (2012) 23793–23802.

[38] E. Grodzka, K. Winkler, B.M. Esteban, C. Kvarnström, Capacitance properties of electrochemically deposited polyazulene films, Electrochim. Acta. 55 (2010) 970–978.

[39] K. Iwasaki, H. Tatematsu, Y. Taneda, K. Matsumoto, S. Hino, Temperature and solvents effects on the electrochemical polymerization of azulene, Synth. Met. 69 (1995) 543–544.

[40] J. Keskinen, S. Lehtimäki, A. Dastpak, S. Tuukkanen, T. Flyktman, T. Kraft, A. Railanmaa, D. Lupo,

Architectural modifications for flexible supercapacitor performance optimization, Electron. Mater. Lett. 12 (2016) 795–803.

[41] C. Lete, B.M. Esteban, C. Kvarnström, A.C. Razus, A. Ivaska, Electrosynthesis and characterization of poly(2-[(E)-2-azulen-1-ylvinyl] thiophene) using polyazulene as model compound, Electrochim. Acta. 52 (2007) 6476–6483.

[42] C. Daguenet, P.J. Dyson, I. Krossing, A. Oleinikova, J. Slattery, C. Wakai, H. Weingärtner, Dielectric Response of Imidazolium-Based Room-Temperature Ionic Liquids, J. Phys. Chem. B. 110 (2006) 12682–12688.

[43] H. Weingärtner, P. Sasisanker, C. Daguenet, P.J. Dyson, I. Krossing, J.M. Slattery, T. Schubert, The Dielectric Response of Room-Temperature Ionic Liquids: Effect of Cation Variation, J. Phys. Chem. B. 111 (2007) 4775–4780.

[44] P. Hapiot, C. Lagrost, Electrochemical reactivity in room-temperature ionic liquids, Chem. Rev. 108 (2008) 2238–2264.

[45] J. Dupont, P.A.Z. Suarez, R.F. De Souza, R.A. Burrow, J.-P. Kintzinger, C-H-π Interactions in 1-n-Butyl-3-methylimidazolium Tetraphenylborate Molten Salt: Solid and Solution Structures, Chem. - A Eur. J. 6 (2000) 2377–2381.

[46] C.A. Brooks, A.P. Doherty, Electrogenerated radical anions in room-temperature ionic liquids, J. Phys. Chem. B. 109 (2005) 6276–6279.

[47] J.G. Huddleston, A.E. Visser, W.M. Reichert, H.D. Willauer, G.A. Broker, R.D. Rogers, Characterization and comparison of hydrophilic and hydrophobic room temperature ionic liquids incorporating the imidazolium cation, Green Chem. 3 (2001) 156–164.

[48] A.J.L. Costa, M.R.C. Soromenho, K. Shimizu, I.M. Marrucho, J.M.S.S. Esperanca, J.N.C. Lopes, L.P.N. Rebelo, Density, thermal expansion and viscosity of cholinium-derived ionic liquids, ChemPhysChem. 13 (2012) 1902–1909.

[49] A.P. Fröba, H. Kremer, A. Leipertz, Density, Refractive Index, Interfacial Tension, and Viscosity of Ionic Liquids [EMIM][EtSO4], [EMIM][NTf2], [EMIM][N(CN)2], and [OMA][NTf2] in Dependence on Temperature at Atmospheric Pressure, J. Phys. Chem. B. 112 (2008) 12420–12430.

[50] R.G. Evans, O. V. Klymenko, C. Hardacre, K.R. Seddon, R.G. Compton, Oxidation of N,N,N',N'-tetraalkyl-para-phenylenediamines in a series of room temperature ionic liquids incorporating the bis(trifluoromethylsulfonyl)imide anion, J. Electroanal. Chem. 556 (2003) 179–188.

[51] G. Nie, T. Cai, S. Zhang, J. Hou, J. Xu, X. Han, Low potential electrosyntheses of high quality freestanding polyazulene films, Mater. Lett. 61 (2007) 3079–3082.

[52] R.M. Latonen, B. Meana Esteban, C. Kvarnström, A. Ivaska, Electrochemical polymerization and

characterization of a poly(azulene)-TiO2 nanoparticle composite film, J. Appl. Electrochem. 39 (2009) 653–661.

[53] G. Nöll, C. Lambert, M. Lynch, M. Porsch, J. Daub, Electronic structure and properties of poly- and oligoazulenes, J. Phys. Chem. C. 112 (2008) 2156–2164.

[54] G.R. Hunt, I.G. Ross, Spectrum of Azulene Part I. Infrared Spectrum, J. Mol. Spectrosc. 3 (1959) 604–620.

[55] X. Chen, H. Lin, J. Deng, Y. Zhang, X. Sun, P. Chen, X. Fang, Z. Zhang, G. Guan, H. Peng, Electrochromic fiber-shaped supercapacitors, Adv. Mater. 26 (2014) 8126–8132.

[56] D. Weingarth, A. Foelske-Schmitz, R. Kötz, Cycle versus voltage hold - Which is the better stability test for electrochemical double layer capacitors?, J. Power Sources. 225 (2013) 84–88.

[57] V. Khomenko, E. Frackowiak, F. Béguin, Determination of the specific capacitance of conducting polymer/nanotubes composite electrodes using different cell configurations, Electrochim. Acta. 50 (2005) 2499–2506.

[58] A. Laforgue, All-textile flexible supercapacitors using electrospun poly(3,4- ethylenedioxythiophene) nanofibers, J. Power Sources. 196 (2011) 559–564.

[59] T. Brousse, D. Bélanger, D. Guay, Asymmetric and Hybrid devices in Aqueous Electrolytes, in: Supercapacitors Mater. Syst. Appl., 2013: pp. 257–288.